Asian Journal of Pharmaceutical Sciences 15 (2020) 326–335

Available online at www.sciencedirect.com

ScienceDirect

journal homepage: www.elsevier.com/locate/AJPS

Original Research Paper

Intranasal delivery of paeoniflorin nanocrystals for brain targeting

Chaoyin Wu[a], *Benyue Li*[a], *Yi Zhang*[a], *Tingting Chen*[b], *Chuangrong Chen*[c], *Wei Jiang*[d], *Qi Wang*[a,*], *Tongkai Chen*[a,*]

[a] *Institute of Clinical Pharmacology, Guangzhou University of Chinese Medicine, Guangzhou 510405, China*
[b] *Guangzhou Institutes of Biomedicine and Health, Chinese Academy of Sciences, Guangzhou 510530, China*
[c] *Science and Technology Department, Guangzhou University of Chinese Medicine, Guangzhou 510006, China*
[d] *Department of Radiology, Sun Yet-sen Memorial Hospital, Sun Yet-sen University, Guangzhou 510120, China*

ARTICLE INFO

Article history:
Received 12 June 2019
Revised 27 August 2019
Accepted 7 November 2019
Available online 26 November 2019

Keywords:
Intranasal delivery
Nanocrystals
Paeoniflorin
Brain targeting
Neuroprotective effect

ABSTRACT

Paeoniflorin (PA) is an anti-Parkinson Chinese medicine with inferior bioavailability and difficulty in delivery to the brain. This research is to develop an efficacious PA nanocrystal formulation (PA-NCs) that is suitable for intranasal administration to treat Parkinson's disease (PD). PA-NCs were fabricated through an antisolvent precipitation method using TPGS as the stabilizer. The rod-shaped PA-NCs had particle size of 139.6 ± 1.3 nm and zeta potential of −23.2 ± 0.529 mV. A molecular dynamics simulation indicated that van der Waals forces are the primary drivers of interactions between PA and TPGS. In the *ex vivo* nasal mucosa permeation assay, the cumulative drug release at 24 h was 87.14% ± 5.34%, which was significantly higher than that of free PA. PA-NCs exhibited substantially improved cellular uptake as well as permeability on Calu-3 cells as compared to PA alone. FRET imaging analysis demonstrated that intact NCs could be internalized into Calu-3 cells. Moreover, PA-NCs conferred desirable protective effect against MPP^+-induced SH-SY5Y cellular damage. Pharmacokinetic studies revealed a higher PA concentration in the brain following intranasal delivery of PA-NCs. In summary, the intranasal administration of PA-NCs is a promising treatment strategy for PD.

1. Introduction

Paeoniflorin (PA) is an active constituent of *Paeonia lactiflora* Pall. roots, which have been extensively utilized as a medicine in China for thousands of years. Numerous studies have revealed the multiple pharmacological activities of PA, such as neuroprotective effects [1,2], anti-thrombotic activity [3], regulation of the immune function [4], and antitumor [5,6]. Recently, its therapeutic applications in Parkinson's disease

* Corresponding author. Institute of Clinical Pharmacology, Guangzhou University of Chinese Medicine, 12 Jichang Road, Guangzhou 510405, China. Tel.: +86 20 36585066.
E-mail addresses: wangqi@gzucm.edu.cn (Q. Wang), chentongkai@gzucm.edu.cn (T.K. Chen).
Peer review under responsibility of Shenyang Pharmaceutical University.

https://doi.org/10.1016/j.ajps.2019.11.002

(PD) have been gaining increasing attention. For instance, it was established that PA delayed dopamine-neuronal damage and attenuated the reduction of dopamine and its metabolites in a rat PD model induced by 6-hydroxydopamine (6-OHDA) [1] or 1-methyl-4-phenyl-1,2,3,6-tetrahydropyridine (MPTP) [2]. The neuroprotective effects of PA are mediated by upregulating bcl/bax ratio and reducing the expression of caspase-3 [7]. However, the log *P* value of PA is −2.88, which leads to poor permeation by passive diffusion and low bioavailability [8]. The apparent volume of distribution after intravenous administration (18 mg/kg) in rats was only 1.33 ± 0.24 l/kg [9]. As a consensus, blood-brain barrier (BBB) preserves the brain against noxious circulating substances as well as drugs [10]. PA was poorly absorbed in MDCK-MDR1 cell monolayers (an *in vitro* BBB model) because its efflux ratio was higher than 2.0 when the treated concentration of PA was between 100 and 800 μg/ml [11].

Different nanomedicine systems have been designed to enhance the permeability of compounds with undesirable bioavailability. Among them, drug nanocrystals (NCs) are made from almost 100% drugs stabilized by surfactants or polymeric steric stabilizers, so that they can carry a higher percentage of drugs than other polymeric carrier systems [12]. Typically, the NCs improve dose-bioavailability proportionality, as well as reduce drug toxicity and side effects [13]. A major concern is that NCs targeting the BBB rather than mononuclear phagocytic system (MPS) needs to escape the immune system first. Also, the *in vivo* circulation time should be shortened to enhance the brain targeting efficiency of NCs to avoid their dissolution in the blood [12]. Consequently, changing the administration route of NCs might be a potential strategy.

Intranasal drug administration is an effective approach for directly targeting the brain via olfactory and trigeminal neural systems bypassing the BBB. Thus, intranasal administration hinders drug loss from the first-pass effect and ensures faster onset of pharmacological activity [14]. When a drug is administered to olfactory mucosa region, it transports either transcellularly or paracellularly through the mucous layer [15]. It was established that the residence time of nanocarriers on nasal mucosa is longer than that of liquid formulations because the latter washed out with mucociliary clearance more easily [16]. Therefore, combining the advantages of NCs and intranasal administration results in significantly amplified contact area with mucosa, extended residence time, superior interaction with tissue or cell surfaces and enhanced drug absorption [17]. Additionally, the intracellular integrity of NCs are incompletely investigated. Accordingly, we entrapped a Förster resonance energy transfer (FRET) pair of fluorophores, DiO (3,3′-dioctadecyloxacarbocyanine perchlorate) as donor and DiI (1,1′-dioctadecyl-3,3,3′,3′-tetramethylindocarbocyanine perchlorate) as acceptor into NCs to monitor their intracellular integrity.

Based on the above knowledge, the purpose of the present study was to prepare and describe paeoniflorin nanocrystals (PA-NCs), which will both enhance its permeation through mucosa and evade BBB, so as to increase the brain concentration of PA. In this study, the antisolvent precipitation method was applied to fabricate PA-NCs. The resulting PA-NCs were further explored by physiochemical characterization, assays of permeation, cellular uptake and transport, FRET imaging analysis, and pharmacological activity studies.

2. Materials and methods

2.1. Materials

PA (purity > 99%) was sourced from Chengdu Preferred Biological Technology Co., Ltd. (Chengdu, China). d-α-tocopheryl polyethylene glycol 1000 succinate (TPGS), 3-(4,5-dimethylthiazolyl)−2,5-diphenyltetrazolium bromide (MTT) and 1-methyl-4-phenylpyridinium ion (MPP^+) were acquired from Sigma-Aldrich (USA). Calu-3 and SH-SY5Y cell lines were acquired from the American Type Culture Collection (USA). Minimum essential medium (MEM) and fetal bovine serum (FBS) were prepared from Gibco (USA). High-performance liquid chromatography (HPLC)-grade acetonitrile, phosphoric acid, formic acid, and phosphotungstic acid were from Shanghai Aladdin biochemical Technology Co., Ltd. (Shanghai, China). DiO and DiI were purchased from Beyotime (China).

2.2. Preparation of PA-NCs

PA-NCs were fabricated using the anti-solvent precipitation technique [18]. Briefly, 1 ml acetone containing 20 mg/ml PA was rapidly injected into 10 ml H_2O including 0.5 mg/ml hydroxypropyl methylcellulose E3 (HPMC E3) under 1000 r/min stirring. To investigate the impact of parameters on size distribution and polydispersity index (PDI), PA-NCs were optimized through a single factor test, containing the types (HPMC E3, Poloxamer 188 (F68), TPGS, Polyvinylyprrolidone (PVP) K30, and sodium dodecyl sulfate (SDS)) and the concentrations (0.1, 0.2, 0.5, 1.0, and 1.5 mg/ml) of stabilizers, the concentrations of PA (10, 20, 30, 40, and 50 mg/ml) and the ratios of anti-solvent-to-solvent (10:1, 20:1, 30:1, 40:1, and 50:1).

2.3. Characterization of PA-NCs

2.3.1. Particle size, PDI and zeta potential

The particle dimensions and PDI of PA-NCs were obtained utilizing a Zetasizer Nano ZS90 (Malvern Instruments Ltd., UK) at 25 °C and 90° scattering angle after proper dilution. Zeta potential of PA-NCs was determined with disposable zeta cells using the electrophoretic mobility technique.

2.3.2. Morphology

The morphology of PA-NCs was observed using the transmission electron microscope (TEM) with an H-7650 camera setup (Hitachi Ltd., Tokyo, Japan). In brief, a droplet of PA-NCs was carefully placed on a grid coated with carbon and stained negatively using phosphotungstic acid (2%, w/v) for 30 s. Subsequently, surplus fluid was deleted and the grid surface was air dried prior to being loaded on the microscope.

2.4. Study of in vitro dissolution

The *in vitro* dissolution of PA-NCs was investigated using dialysis method. In brief, we added 1 ml of PA, PA-NCs, or physical mixture (PA + TPGS, PA-PM) to a 3.5 kDa MWCO

dialysis bag with 50 ml of dialyzing media (phosphate buffer pH 6.8, equal to the pH of nasal fluid). All samples involved the placement in a thermostatic incubator (37 °C) and were shaken at 100 r/min. At defined time points, we removed 1 ml of the dialysis media, with an equal volume of fresh media being added to replace it. After that, PA was detected using HPLC system [19,20]. An Agilent 1100 series HPLC (Santa Clara, USA) workstation was used with a DAD detector, an auto-sampler, and an Ecosil C_{18} (4.6 mm × 250 mm, 5 µm) analytical column. Samples (20 µl) were injected into the HPLC system with mobile phase 0.1% phosphoric acid/acetonitrile (86:14) at 1 ml/min and detected at 230 nm.

2.5. *Molecular dynamics simulation (MDS)*

We set up the PA and TPGS molecules according to MMFF94x Force Field parameters [21]. Using Gaussian09 software, atoms were optimized and the partial atomic charges were calculated. After the addition of Na^+/Cl^- counterions, the complex was solvated in a cuboid box (10 Å) of TIP3P H_2O molecules. Subsequently, MDS was carried out using AMBER16. Based on a previous method, energy minimization was conducted in 2 steps [22]. We finally used the CPPTRAJ program to analyze the trajectories.

2.6. *Ex vivo nasal transmucosal permeation*

Porcine nasal mucosa acquired from a slaughterhouse was stored at −80 °C in 10% formalin. Before the test, the mucosa was allowed to attain ambient temperature and placed between the receiver and donor compartments of a Franz diffusion cell [23]. It was stabilized by running fresh dissolution media 10 times at 37 ± 1 °C. PA-NCs or PA (1 ml) were put into each compartment of donor, and the specimens in the receiver compartments were collected at 0, 0.25, 0.5, 1, 2, 4, 8, 12 and 24 h. The PA concentrations in all samples were then determined by means of HPLC described in Section 2.4. The release data were fitted to zero-order, first-order, Peppas and Higuchi release models [24]. Initial equations Eqs. 1–4 for various models were given below:

$$\text{Zero} - \text{order model} : Q_r = Q_0 + Kt \quad (1)$$

$$\text{First} - \text{order model} : \ln Q_r = \ln Q_0 + Kt \quad (2)$$

$$\text{Korsmeyer} - \text{Peppas model} : Q_t/Q_\infty = Kt^n \quad (3)$$

$$\text{Higuchi model} : Q_t = K(t)^{1/2} \quad (4)$$

Where Q_t is the drug released quantity in time t, Q_0 is the primary quantity, and K is the constant of drug release rate.

2.7. *In vitro cellular uptake and transport in Calu-3 cells*

2.7.1. *Cell culture*

Calu-3 cells were utilized as *in vitro* nasal platforms for the first time to evaluate microparticles and polymer gel for protein delivery [25], and this cell line has been utilized as a nasal epithelium model by more and more researchers [26]. The Calu-3 cells were cultured in 10% FBS, 100 U/ml penicillin, and 100 µg/ml streptomycin in a humid air with 5% CO_2 at 37 °C. When the cells attained 90% confluence, they were trypsinized by means of 0.25% trypsin and 0.1% ethylenediamine-tetraacetic acid to conduct the subsequent studies, including cytotoxicity assays, cellular uptake and transportation evaluation.

2.7.2. *Cytotoxicity evaluation*

The Calu-3 cells were implanted into a 96-well plate in 100 µl medium (1×10^5 cells/ml) and incubated as per the above conditions for 24 h. Then, fresh medium containing different concentrations of PA-NCs or PA replaced the previous medium to acquire the ultimate concentrations of 5, 10, 20, 50, 100 and 200 µM. After an additional 12 h or 24 h, 10 µl MTT was added in phosphate-buffered saline (PBS) and incubated for 4 h at 37 °C. Further, 100 µl DMSO was introduced and the absorbance was evaluated at 490 nm by means of a micro-plate multi-detection instrument. The mean absorbance (A) of three wells for each concentration was utilized to measure the viability (%) using the following equation:

$$\text{Viability\%} = \frac{A_{\text{sample}} - A_{\text{blank}}}{A_{\text{control}} - A_{\text{blank}}} \times 100 \quad (5)$$

2.7.3. *Cellular uptake*

The cellular uptake of PA-NCs from the cell lysate was executed to detect an absolute total concentration of PA [27]. In brief, Calu-3 cells were implanted in a 6-well plate (1×10^6 cells/well), treated under the conditions as described above for 24 h and further incubated with PA or PA-NCs or PA-PM (equivalent PA concentration: 20 µM) for 2 h. Next, the culture medium was eliminated and cells were washed with cold PBS (pH 7.4) thrice. After incubation with the cell lysis buffer (1 ml) for 30 min, the entire solution was centrifuged with 20 ml phosphoric acid for 10 min at 12 000 rpm/min. Finally, 20 µl supernatant was used to measure the PA content by HPLC.

2.7.4. *Transport experiment*

Calu-3 cells were seeded (1×10^5 cells/ml) onto collagen-coated transparent PET Transwell membranes (0.4 µm, 12 mm), and 1.5 ml medium was introduced into the basolateral chamber. The medium on the upper surface was removed on the fifth day and the transepithelial electrical resistance (TEER) was investigated. The medium in the basolateral chamber was changed every other day. When the cells reached maximum confluence and the TEER values amplified to 500 Ω cm^2, polarized cell monolayers were formed. After removing the medium, the cells were washed thrice with Hank's balanced salt solution (HBSS) and balanced at 37 °C for 30 min. PA or PA-PM or PA-NCs suspension (500 µl; containing 20 µM PA) and HBSS (1.5 ml) were placed onto the apical (A) and basolateral (B) sides to estimate the A→B transport. Two hours later, 500 µl samples were obtained from the B side and the quantity of PA transported was measured using HPLC. The apparent permeability coefficient (P_{app}) for PA was estimated based on the following equation:

$$P_{app} = \frac{(dQ/dt)}{CS} \quad (6)$$

where dQ/dt denotes the rate of apparent appearance of PA in the receptor side; C denotes the PA concentration in the chamber of donor; S denotes the membrane surface area.

2.8. Examination of FRET imaging

The intracellular integrity of NCs in Calu-3 cells was examined by means of FRET imaging. DiO and DiI was entrapped into PA-NCs (DiO/DiI/PA-NCs) employing the same method of PA-NCs preparation. The FRET signals of DiO/DiI/PA-NCs diluted in acetone and water are evaluated at 420 nm excitation wavelength and 485–650 nm emission wavelengths. Calu-3 cells were treated with DiO/DiI/PA-NCs at 20 μM PA at 37 °C for two different incubation times (0.5 and 1 h). After incubation, the culture medium was eliminated, and the cells were washed twice with cold PBS. They were then stabilized in 4% paraformaldehyde and investigated by confocal laser scanning microscopy.

2.9. PA-NCs protection against MPP^+-mediated cytotoxicity

2.9.1. Cell culture

SH-SY5Y cells were grown in medium consisting of 10% FBS, penicillin (100 U/ml) and streptomycin (100 μg/ml) at 37 °C in an atmosphere of 5% CO_2 and 95% relative humidity.

2.9.2. Cell viability assay

The cells were implanted in a 96-well plate (5000 cells/cm^2) and left for 24 h to attach. They were pretreated with PA-NCs (5, 10 and 30 μM) and an equal dose of PA or 0.1% DMSO for 2 h, incubated with 2 mM MPP^+ for 36 h, and further incubated with 10% (v/v) MTT solution (5 mg/ml) for 4 h. Intracellular formazan was solubilized using DMSO and the absorbance was acquired at 570 nm.

2.9.3. Measuring intracellular ATP level

Intracellular ATP of SH-SY5Y cells was quantified by means of an ATP Assay Kit (Beyotime Biotechnology). The cells were pretreated with PA-NCs (5, 10 and 30 μM) and an equal dose of PA or 0.1% DMSO for 2 h, then incubated with 2 mM MPP^+ for 36 h, after which they were washed and lysed with 200 μl of lysis buffer. The ATP concentration was measured by means of a standard curve (1 nM to 10 μM) and normalized to protein concentrations by means of the BCA Protein Assay Kit (Beyotime Biotechnology).

2.9.4. Measuring mitochondrial membrane potential (MMP)

MMP was characterized utilizing JC-1 MMP assay kit (Beyotime Biotechnology). In summary, the cells were pretreated with PA-NCs (5, 10 and 30 μM) and an equal dose of PA or 0.1% DMSO for 2 h, incubated with 2 mM MPP^+ for 36 h. Then, the cells were washed and treated with the pre-prepared JC-1 solution based on the manufacturer's instructions.

2.10. Pharmacokinetic analysis of PA-NCs in rats

The protocol of animal for rats was accepted by the Animal Ethics Committee of Guangzhou University of Chinese Medicine based on the national regulatory principles. Male Sprague-Dawley (SD) rats with age of 6–8 weeks were sourced from the Guangdong Medical Laboratory Animal Centre. They were kept in a temperature-, humidity- and light-controlled environment, under 12-h night/12-h dark situations with free access to food and water. The rats were divided into two groups: Intravenous administration (IV) group and intranasal administration (IN) group, and each group contained 6 rats for the plasma pharmacokinetic study. PA-NCs (dose 1.2 mg/kg) were administered intravenously or intranasally to each group, respectively. For IN group, 105 ± 3 μl of PA-NCs was pipetted into the nasal cavity of the left nostril (single nostril) over 4 min to make sure that PA-NCs was delivered into the nasal cavity. The blood and brain specimens of treated rats were gathered individually. Blood samples were collected (300 μl each) via posterior orbital venous plexus at specific time intervals (before and at 0.083, 0.25, 0.5, 1, 2, 3, 4, 6, and 8 h after administration) and were centrifuged at 5000 rpm for 10 min. 200 μl of the serum supernatant were blended with 190 μl of the acetonitrile and spiked with 10 μl of the acetonitrile including 1 μg/ml of geniposide (an internal standard).

In the brain pharmacokinetic study, four rats were included in the IV group and the IN group, respectively. After administration, the rats were killed by cervical dislocation at various time intervals as mentioned above. Subsequently, cardiac perfusion was carried out with 30 ml normal saline. Ultimately, the rat was beheaded, and the entire brain was eliminated, weighed, and homogenized in pre-cooled saline at a ratio of 1:2 (w/v). 200 μl of the homogenized brain samples were blended with 190 μl of the acetonitrile and spiked with 10 μl of the acetonitrile including 1 μg/ml of bifendate.

The concentrations of PA in the plasma and brain were evaluated using a Q-Trap 4000 MS/MS system (Applied AB Sciex, USA) coupled to an Agilent 1100 series HPLC system. The chromatographic purification was performed using an Ecosil C18 analytical column. The mobile phase was acetonitrile and 5 mM ammonium acetate buffer consisting of 0.05% formic acid (20:80, v/v), at 200 μl/min with 5.0 min per specimen. The MS/MS was detected by controlling the fragmentation of m/z 498.2→179.1 for PA and 406.2→227.1 for the internal standard geniposide. The maximum concentration (C_{max}), the time to attain the maximum concentration (T_{max}) and area under the curve (AUC) of PA in plasma or in the brain were calculated utilizing Drug and Statistics software version 2.0. The pharmacokinetic profiles were constructed by plotting drug concentration *versus* time curves. Furthermore, the PA-NCs targeting efficiency (DTE) and direct transport percentage (DTP) were estimated using the following equation [23]:

$$\mathrm{DTE\%} = \frac{[AUC_{\mathrm{Brain}}/AUC_{\mathrm{Blood}}]^{(\mathrm{IN})}}{[AUC_{\mathrm{Brain}}/AUC_{\mathrm{Blood}}]^{(\mathrm{IV})}} \times 100 \quad (7)$$

$$\mathrm{DTP\%} = \frac{B_{\mathrm{IN}} - B_{\mathrm{X}}}{B_{\mathrm{IN}}} \times 100 \quad (8)$$

in which $Bx = (B_{IV}/P_{IV}) \times P_{IN}$, Bx denotes the brain AUC traction from circulation through BBB after intranasal delivery, B_{IV} denotes the AUC_{0-8h} (brain) after intravenous delivery, P_{IV} denotes the AUC_{0-8h} (blood) after intravenous delivery, B_{IN}

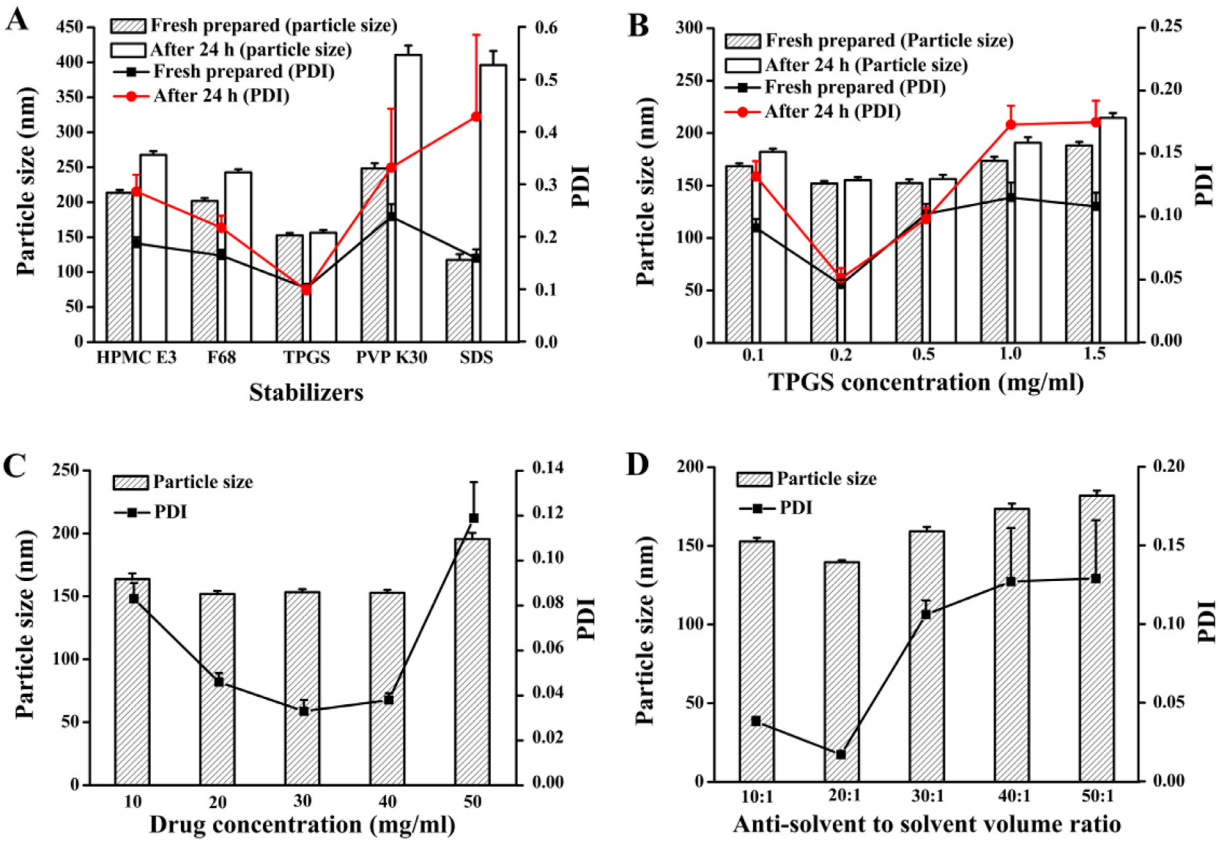

Fig. 1 – Optimal parameters based on particle size and PDI of PA-NCs ($n = 3$). (A) Stabilizers (at the concentration of 0.5 mg/ml); (B) TPGS concentration; (C) drug concentration; (D) antisolvent to solvent volume ratio.

denotes the AUC_{0-8h} (brain) after intranasal delivery and P_{IN} denotes the AUC_{0-8h} (blood) after intranasal delivery.

2.11. *Statistical analysis*

The statistical differences between two groups and more than two groups were analyzed by two-tailed independent sample *t*-test and one-way analysis of variance (ANOVA), respectively. All results are presented as means ± SD. A probability of *P* less than 0.05 was considered statistically significant.

3. Result and discussion

3.1. *Preparation and characterization of PA-NCs*

The particle size and PDI of the PA-NCs prepared with TPGS as the stabilizer were 152.4 ± 3.6 nm and 0.102 ± 0.008, respectively (Fig. 1A). It was observed that PA-NCs exhibited the smallest size and PDI when stabilized by TPGS. After 24 h, the particle size and PDI were 156.3 ± 3.9 nm and 0.098 ± 0.009, respectively, indicating that the PA-NCs have neither dissociated nor aggregated. These results showed that TPGS could make PA-NCs more stable than the other excipients when the stirring speed, drug concentration and the antisolvent to solvent volume ratio were the same. To illustrate the impact of the stabilizer on the fixation of the NCs, the solubility of PA with each stabilizer (HPMC E3, F68, TPGS, PVP K30, or SDS) has been examined. The solubility of PA was not increased when utilizing HPMC E3, F68, PVP K30, or SDS as stabilizer. However, when utilizing TPGS as a stabilizer, the aqueous solubility of PA was improved at less 3.6-fold in comparison to the solubility of the raw PA. The minimum particle size, lowest PDI and greatest stability were expressed when the concentration of TPGS was 0.2 mg/ml (Fig. 1B). Using 0.2 mg/ml TPGS with 1000 rpm stirring speed at ambient temperature, as the concentration of PA were 20, 30, 40 mg/ml, the particle size of PA-NCs were 151.9 ± 2.4 nm, 153.2 ± 2.5 nm, 152.8 ± 2.3 nm, respectively and the PDI were 0.046 ± 0.004, 0.033 ± 0.005, 0.038 ± 0.003, respectively. There was no remarkable difference between the three concentrations (Fig. 1C). In consideration of maximum drug in this formulation, 40 mg/ml PA was chosen as the optimal drug concentration. Finally, the various ratios of anti-solvent to solvent volume was compared based on particle size and PDI under the above determined situations (Fig. 1D). The optimal conditions for the preparation of the PA-NCs include injecting 40 mg/ml PA in acetone (solvent) into 0.2 mg/ml TPGS in water (antisolvent) at 20:1 antisolvent/solvent volume ratio while stirring at 1000 rpm. The particle size, PDI and zeta potential of the resulting PA-NCs were 139.6 ± 1.3 nm, 0.013 ± 0.002 and −23.2 ± 0.529 mV, respectively (Fig. 2A and 2B). The PA-NCs

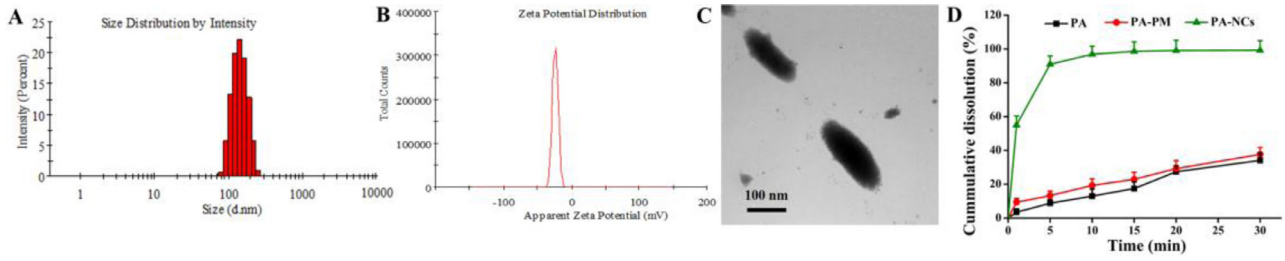

Fig. 2 – Characterization of PA-NCs. (A) Particle size. (B) Zeta potential. (C) TEM. (D) Dissolution profiles of PA powder, physical mixture of PA and TPGS (PA-PM) and PA-NCs in phosphate buffer (pH 6.8, $n = 3$).

were stable for at least 2 weeks with the mean particle size and distribution remaining unchanged (Table S1). As shown in Fig. 2C, using a transmission electron microscope (TEM), the PA-NCs were rod-shaped with a length of 90–150 nm, which was accordant with the average diameter achieved from dynamic light scattering (DLS). The dissolution profiles of PA-NCs, physical mixture of PA and TPGS (PA-PM) and PA powder were compared (Fig. 2D). It was observed that more than 90% of PA was quickly released from NCs within 5 min. However, less than 40% of PA was released after 30 min from the PA powder or the PA-PM. The enhanced rate of dissolution was possibly due to the decrease of the particle size and the increase of surface area of the PA-NCs as explained by the Noyes–Whitney equation [12].

3.2. *Molecular dynamics simulation (MDS)*

MDS of PA and TPGS in water was carried out to investigate the binding interactions and energy. Fig. 3A shows the conformations of PA and TPGS at 0, 12.5, 24 and 25.5 ns. The distances time evolution revealed unplanned interaction between PA and TPGS starting from ~11 ns (Fig. 3B). After the interaction, they stayed in a constant complex until ~23.5 ns. A brief break in the interaction between PA and TPGS was detected from ~24 ns to ~24.5 ns of the simulation, and then the interaction was reestablished and remained stable until the end. The interaction energy time evolution between the PA and TPGS is shown in Fig. 3C and the mean interaction energy was ~−56.16 kJ/mol from 11 to 40 ns. The contribution to the binding free energy (ΔG_{total}) from the vdW and electrostatic interactions was denoted by ΔE_{vdw} and ΔE_{elec}, whereas the polar and nonpolar solvation energies were denoted by ΔG_{polar} and $\Delta G_{nonpolar}$, respectively. The PA-TPGS binding mainly involved hydrophobic interactions, with ΔE_{vdW} being the greatest contributor. ΔG_{polar} was inadequate for the binding, while $\Delta G_{nonpolar}$ was favorable, which resulted in favorable binding energy. ΔG_{total} calculated using the MM-PBSA method from 11 ns to 40 ns was found to be -35.729 ± 0.521 kJ/mol (Table 1).

3.3. *Ex vivo nasal mucosa permeation*

Ex vivo investigations were performed to assess the permeation of the PA-NCs across the porcine nasal mucosa. The curves illustrated that PA-NCs permeated faster than PA from 5 min to 24 h. The cumulative drug permeation of PA-NCs at 24 h was 87.14% ± 5.34%, while less than 25% of PA permeated from the PA powder (Fig. 4). The different permeation characteristics indicated that PA-NCs could penetrate the mucosal barrier more easily than free PA. It may be attributed to the amphipathic nature of TPGS which makes it a bioavailability enhancer [28]. The parameters of permeation data fitted to various mathematics models are shown in Fig. S1 and Table S2. The model with the determination of coefficient (R^2) closest to 1 was regarded as the drug release model [29]. As was evident from Table 2, the release of PA-NCs significantly correlated with first-order and Higuchi models whose R^2 values were 0.95528 and 0.95168, respectively. The release of PA inclined to Higuchi model since its R^2 value was 0.93718. As the 'n' values of PA-NCs and PA (PA-NCs: 0.48402; PA: 0.47885) were between 0.5 and 1, we concluded that the release mechanism of PA-NCs and PA was anomalous transport (non-Fickian model) based on Peppas' theory [29,30].

Table 1 – Energies of the PA-TPGS complex from the MM-PBSA calculations. Data are acquired from three various simulations and exhibited as means ± SD ($n = 3$).

Component	Energy (kJ/mol)
ΔE_{vdw}	-49.655 ± 0.664
ΔE_{elec}	-5.499 ± 0.451
ΔG_{polar}	25.619 ± 0.591
$\Delta G_{nonpolar}$	-6.186 ± 0.087
ΔG_{total}	-35.729 ± 0.521

3.4. *Cellular uptake and permeation evaluation*

Calu-3 cells were chosen as the *in vitro* model of nasal mucosa since they were used to investigate nasal drug transportation [31]. An appropriate concentration of PA-NCs for cell transportation and uptake studies was selected via the *in vitro* cytotoxicity assay. The results showed that there was no obvious toxicity on Calu-3 cells incubated for 12 h and 24 h with the concentrations of PA or PA-NCs from 5 to 200 μM (Fig. S2). Calu-3 cells were incubated with 20 μM PA-NCs or PA-PM or PA for 2 h. The P_{app} (A→ B) of PA-NCs was $2.48 \pm 0.21 \times 10^{-5}$ cm/s, which was

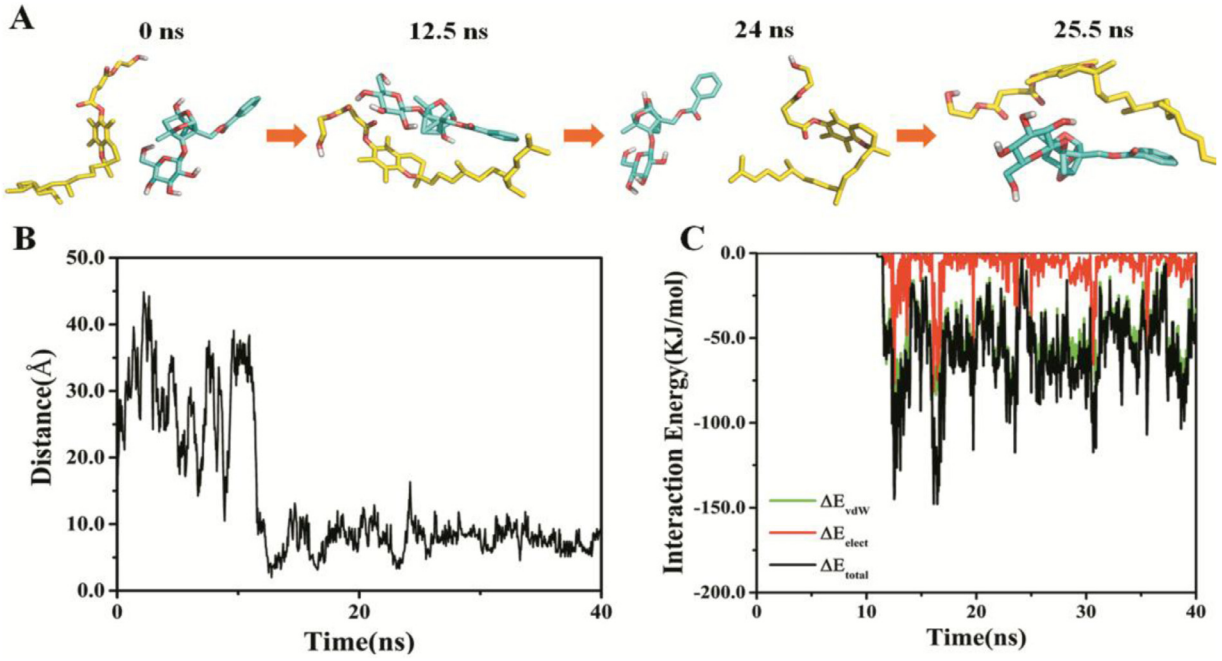

Fig. 3 – MDS of PA and TPGS in the presence of H_2O molecules. (A) PA and TPGS structures of at 0, 12.5, 24 and 25.5 ns. TPGS is illustrated in yellow, while PA is illustrated in cyan. (B) Distances between centers of mass of GA and TPGS over time. (C) Time evolution of interaction energy between PA and TPGS. (For interpretation of the references to color in this figure legend, the reader is referred to the web version of this article.)

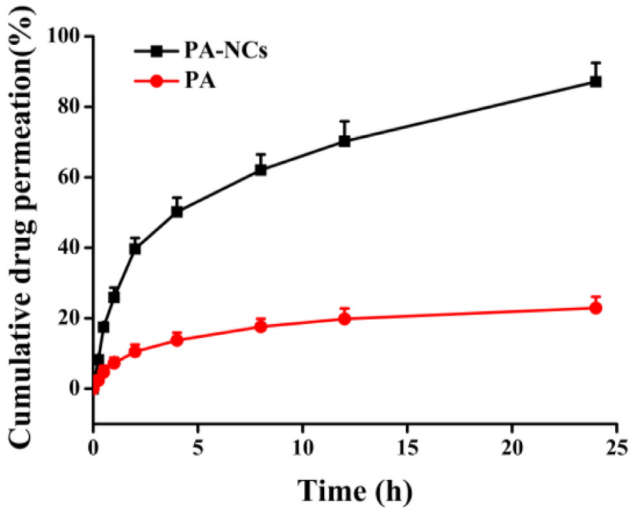

Fig. 4 – *Ex vivo* nasal mucosa permeation profile of PA-NCs and PA ($n = 3$).

Table 2 – Pharmacokinetic parameters after administration of PA-NCs at 1.2 mg/kg. Data are represented as means ± SD.

Parameters	Intravenous	Intranasal
Plasma		
$T_{1/2}$ (h)	0.099 ± 0.016	0.33 ± 0.09**
T_{max} (h)	0.083 ± 0	0.33 ± 0.13
C_{max} (ng/ml)	169.58 ± 20.72	29.68 ± 3.05**
$AUC_{0\text{-}t}$ (ng h/ml)	77.44 ± 8.38	44.65 ± 5.17**
$MRT_{0\text{-}t}$ (h)	1.78 ± 0.16	1.65 ± 0.12*
Brain		
$T_{1/2}$ (h)	1.55 ± 0.24	1.16 ± 0.18
T_{max} (h)	0.38 ± 0.14	0.67 ± 0.29*
C_{max} (ng/g)	47.19 ± 5.69	108.47 ± 9.5**
$AUC_{0\text{-}t}$ (ng h/g)	94.11 ± 10.37	230.86 ± 18.56**
$MRT_{0\text{-}t}$ (h)	2.71 ± 0.11	2.67 ± 0.13
Brain/plasma ratio		
DTE	416.60%	
DTP	76.50%	

$n = 6$ or 4, *$P < 0.05$ and **$P < 0.01$ *vs* intravenous group.

higher than that of PA and PA-PM ($0.47 \pm 0.09 \times 10^{-5}$ and $0.53 \pm 0.07 \times 10^{-5}$ cm/sec, respectively). In the PA-NCs group, there was 2.56 ± 0.19 μg PA/mg protein of Calu-3 cells, which was the highest among the three treatment groups, followed by PA-PM (1.27 ± 0.14 μg/mg protein). PA whose concentration in Calu-3 cells was only 1.03 ± 0.16 μg/mg protein entered Calu-3 cells less than the other two groups. The results illustrated that TPGS had little benefit on PA transportation across polarized monolayers of Calu-3 cells if it had not been prepared into NCs with PA.

3.5. *FRET imaging analysis*

DiO and DiI were embedded inside PA-NCs to yield DiO/DiI/PA-NCs. DiO/DiI/PA-NCs were fabricated by mixing DiO and DiI at a ratio of 1:1 (0.5% of each to PA), to determine the intracellular integrity. The average particle size of DiO/DiI/PA-NCs was 140.8 ± 1.6 nm with a PDI of 0.017 ± 0.005. The DiO/DiI/PA-NCs were regarded as intact NC if the FRET signal was seen, illustrating that DiO and DiI are available in the same NC. On the contrary, breakdown or release of NCs led to

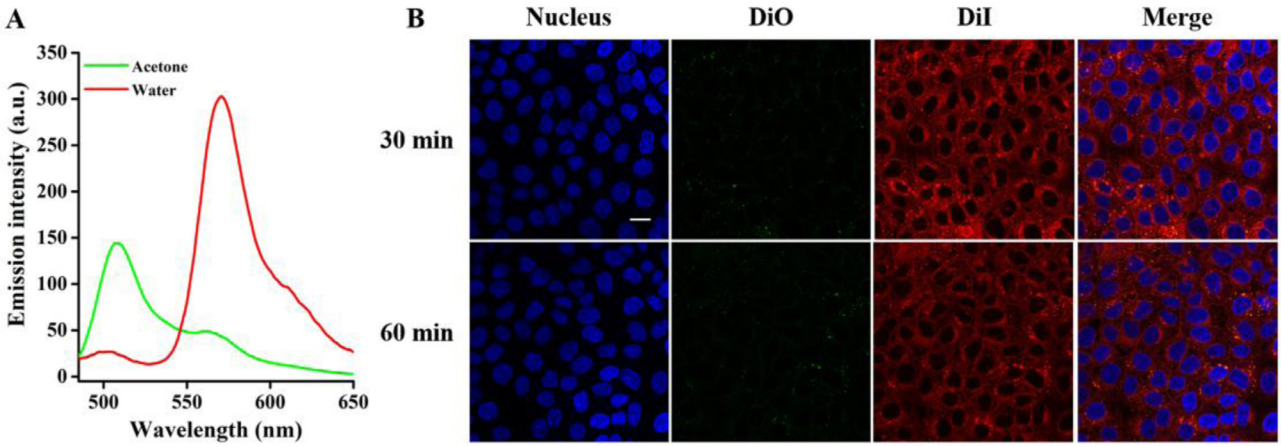

Fig. 5 – Intracellular integrity monitoring by FRET. (A) Green curve represents the fluorescence spectrum of DiO/DiI/PA-NCs diluted in acetone, whereas red curve indicates the DiO/DiI/PA-NCs spectrum diluted in water. (B) Cellular uptake of DiO/DiI/PA-NCs at two different incubation times (0.5 and 1 h). Scale bar: 20 μm. (For interpretation of the references to color in this figure legend, the reader is referred to the web version of this article.)

an absence in the FRET signal because DiO and DiI were separated. As shown in Fig. 5A (red curve), after dispersing the DiO/DiI/PA-NCs in water, a high severity of DiI signal (red fluorescence, FRET ratio of 0.92 ± 0.02) were observed. These findings were probably because of the short interval between DiI and DiO. The peak was changed from 565 to 505 nm, after dissolving DiO/DiI/PA-NCs in acetone, offering that DiI and DiO may be isolated by acetone (Fig. 5A, green curve). To study the intracellular integrity of NCs, Calu-3 cells were treated with DiO/DiI/PA-NCs at 20 μM PA. Importantly, a strong DiI signal and a very low DiO signal (green fluorescence) were observed (Fig. 5B), representing the intracellular integrity of NCs during the treatment. It has been stated that particles with sizes less than 200 nm enter into the cells via clathrin-mediated endocytosis [32]. Therefore, PA-NCs with particle size of 139.6 ± 1.3 nm are taken up into cells via endocytosis mediated by clathrin.

3.6. *PA-NCs protection against MPP^+-mediated cytotoxicity*

MTT analysis revealed 45.34% cell death in SH-SY5Y cells incubated with 2 mM MPP^+. The treatment with 5, 10 and 30 μM of PA-NCs considerably enhanced the viability (71.67%, 87.36% and 97.94%, respectively) of MPP^+-treated cells in a manner based on the dose (Fig. 6). Importantly, PA-NCs displayed more potent neuroprotective activity in reversing MPP^+-induced cytotoxicity than that of PA. Furthermore, the intracellular ATP levels were analyzed to assess the effect of PA-NCs on the energy metabolism of SH-SY5Y cells. As shown in Fig. 7A, treatment with 5, 10 and 30 μM of PA-NCs notably inhibited MPP^+-induced energy deficiency in a dose-dependent mode, from 42.36% to 69.44%, 81.73%, and 95.79%, respectively. Likewise, PA-NCs inhibited MPP^+-induced MMP loss dose-dependently, from 47.51% to 73.52%, 86.71%, and 96.88%, respectively (Fig. 7B).

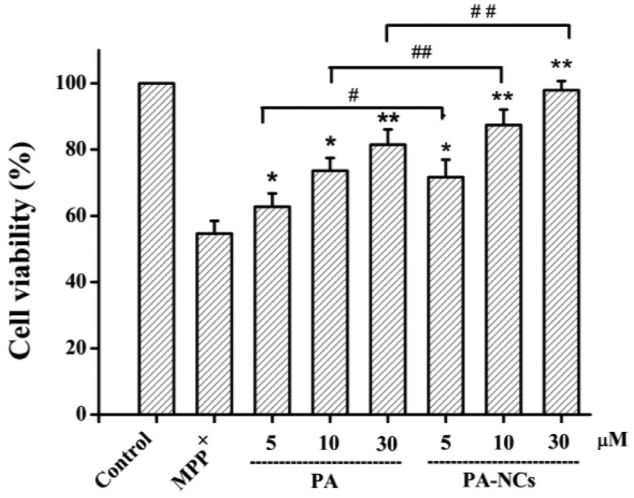

Fig. 6 – Protective effect of PA-NCs towards MPP^+-induced SH-SY5Y cell death. $^*P < 0.05$ and $^{**}P < 0.01$ *vs* MPP^+ group. $^{\#}P < 0.05$ and $^{\#\#}P < 0.01$ *vs* PA treatment group.

3.7. *Pharmacokinetic study*

The curves of the concentrations of PA in plasma and brain *versus* time after intranasal (IN) or intravenous administration (IV) of PA-NCs are shown in Fig. 8. The PA concentrations of IN in plasma were lower than that of IV at different time points as illustrated on Fig. 8A. On the contrary, the PA concentrations of IN in the brain were higher than that of IV from 0.5 to 8 h after administration (Fig. 8B), which indicated that most PA-NCs directly enter the brain via olfactory and trigeminal neural pathways rather than blood circulation after IN. After IV, PA-NCs continuously dissolved in the blood and less PA distributed to the brain due to the BBB. The pharmacokinetic parameters of plasma and brain are listed in Table 2. The $T_{1/2}$, T_{max} and C_{max} after IN in plasma were significantly lower

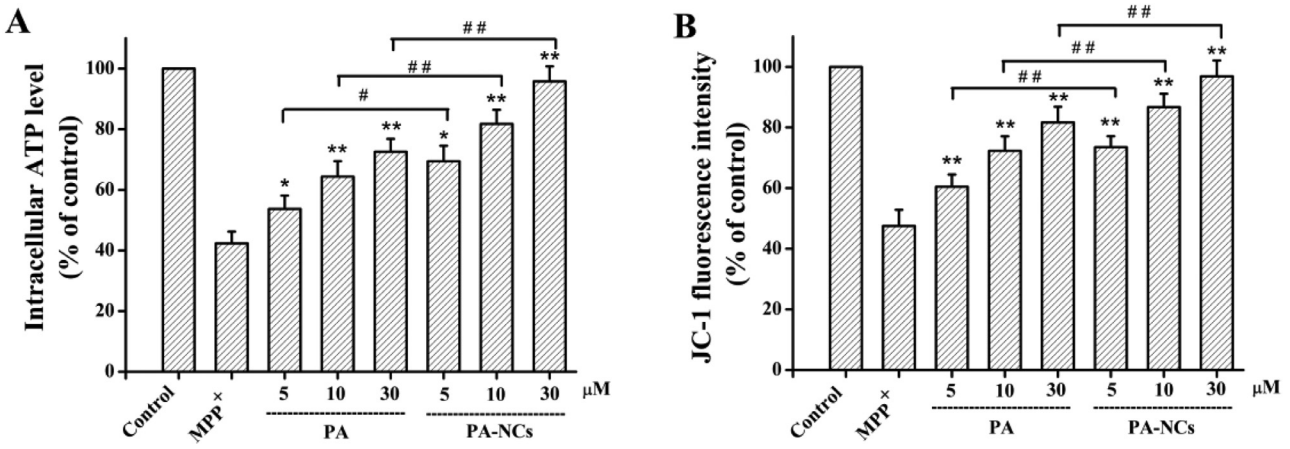

Fig. 7 – Effect of PA-NCs on MPP^+-induced (A) ATP deficiency and (B) mitochondrial membrane potential loss. $^*P < 0.05$ and $^{**}P < 0.01$ vs. MPP^+ group. $^{\#}P < 0.05$ and $^{\#\#}P < 0.01$ vs. PA treatment group.

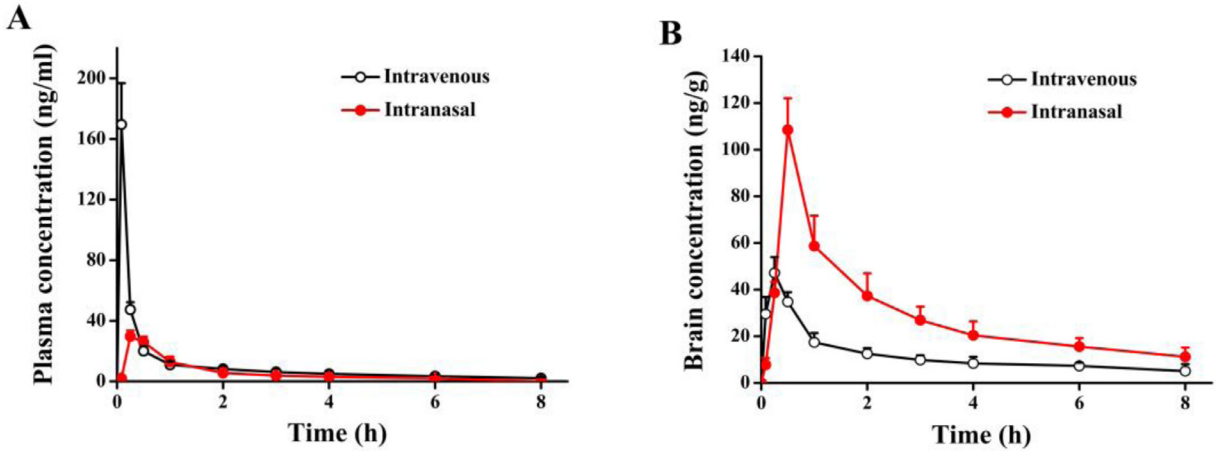

Fig. 8 – Plasma and brain concentrations after IV and IN administration at different time points. (A) Plasma concentration and (B) brain concentration.

than those after IV ($P < 0.01$), whereas the C_{max} after IN in the brain (108.47 ± 9.51 ng/g) was far higher than that after IV (47.19 ± 5.69 ng/g). $AUC_{0\text{-}t}$ is another important parameter that should be considered. While comparing $AUC_{0\text{-}8h}$ (IN) to $AUC_{0\text{-}8h}$ (IV) in the brain, the former (230.86 ± 18.56 ng.h/g) was larger than the latter (94.11 ± 10.37 ng.h/g). These results suggested that IN allows more drugs to bypass BBB into brain without entering the blood circulation. All these results showed that PA-NCs with DTE% and DTP% values of 416.60% and 76.50% could efficiently deliver PA to the brain [33].

4. Conclusions

In this study, stable PA-NCs suitable for intranasal administration were successfully developed with TPGS as the stabilizer using antisolvent precipitation method. MDS revealed that PA and TPGS molecules displayed spontaneous binding in the presence of water molecules, and their bonding mainly depended on van der Waals forces and hydrophobicity. *Ex vivo* permeation studies illustrated that the solubility in physiological solution and biological penetrability of PA-NCs were superior to that of free PA. In addition, PA-NCs obviously enhanced the uptake and transportation of PA in Calu-3 cells. Meanwhile, the intact NCs could be internalized into Calu-3 cells. The higher PA content in the brain validated the targeting efficiency of intranasally delivered NCs. Overall, intranasal administration of PA-NCs can promote the concentration of PA in the brain to a large extent, which might be a promising treatment strategy for PD in the future.

Conflict of interest

The authors report no conflicts of interest.

Acknowledgments

This work was supported by the Guangdong Provincial Natural Science Foundation of China (2018A030310623), the Guangdong Provincial Medical Scientific Research Foundation

of China (A2019027) and the Guangzhou Science Technology and Innovation Commission Technology Research Projects (201805010005).

Supplementary materials

Supplementary material associated with this article can be found, in the online version, at doi:10.1016/j.ajps.2019.11.002.

REFERENCES

[1] Gu XS, Wang F, Zhang CY, Mao CJ, Yang J, Yang YP, et al. Neuroprotective effects of paeoniflorin on 6-OHDA-lesioned rat model of Parkinson's disease. Neurochem Res 2016;41:2923–36.
[2] Zheng MZ, Liu CM, Fan YJ, Yan P, Shi DF, Zhang YC. Neuroprotection by paeoniflorin in the MPTP mouse model of Parkinson's disease. Neuropharmacology 2017;116:412–20.
[3] Dang X, Miao JJ, Chen AQ, Li P, Chen L, Liang JR, et al. The antithrombotic effect of RSNK in blood-stasis model rats. J Ethnopharmacol 2015;173:266–72.
[4] Li PP, Liu DD, Liu YJ, Song SS, Wang QT, Chang Y, et al. BAFF/BAFF-R involved in antibodies production of rats with collagen-induced arthritis via PI3K-Akt-mTOR signaling and the regulation of paeoniflorin. J Ethnopharmacol 2012;141(1):290–300.
[5] Hao J, Yang X, Ding XL, Guo LM, Zhu CH, Ji W, et al. Paeoniflorin potentiates the inhibitory effects of erlotinib in pancreatic cancer cell lines by reducing erbb3 phosphorylation. Sci Rep 2016;6:32809.
[6] Wang ZT, Yu GY, Liu Z, Zhu JW, Chen C, Liu RE, et al. Paeoniflorin inhibits glioblastoma growth *in vivo* and *in vitro*: a role for the TRIAD3A-dependent ubiquitin proteasome pathway in TLR4 degradation. Cancer Manag Res 2018;10:887–97.
[7] Chen AH, Wang HY, Zhang YQ, Wang XY, Yu LS, Xu W, et al. Paeoniflorin exerts neuroprotective effects against glutamateinduced PC12 cellular cytotoxicity by inhibiting apoptosis. Int J Mol Med 2017;40:825–33.
[8] Takeda S, Isono T, Wakui Y, Matsuzaki Y, Sasaki H, Amagaya S, et al. Absorption and excretion of paeoniflorin in rats. J Pharm Pharmacol 1995;47(12A):1036–40.
[9] Wang C, Yuan J, Zhang LL, Wei W. Pharmacokinetic comparisons of Paeoniflorin and Paeoniflorin-6′o-Benzene sulfonate in rats via different routes of administration. Xenobiotica 2016;46(12):1142–50.
[10] Elezaby RS, Gad HA, Metwally AA, Geneidi AS, Awad GA. Self-assembled amphiphilic core-shell nanocarriers in line with the modern strategies for brain delivery. J Control Release 2017;261:43–61.
[11] Hu PY, Liu D, Zheng Q, Wu Q, Tang Y, Yang M. Elucidation of transport mechanism of paeoniflorin and the influence of ligustilide, senkyunolide I and senkyunolide A on paeoniflorin transport through MDCK-MDR1 cells as blood-brain barrier *in vitro* model. Molecules 2016;21(3):300.
[12] Muller RH, Gohla S, Keck CM. State of the art of nanocrystals-special features, production, nanotoxicology aspects and intracellular delivery. Eur J Pharm Biopharm 2011;78(1):1–9.
[13] Wang Y, Zheng Y, Zhang L, Wang Q, Zhang D. Stability of nanosuspensions in drug delivery. J Control Release 2013;172(3):1126–41.
[14] Cunha S, Amaral MH, Lobo JMS, Silvaa AC. Lipid nanoparticles for nasal/intranasal drug delivery. Crit Rev Ther Drug 2017;34(3):257–82.
[15] Khan AR, Liu MR, Khan MW, Zhai GX. Progress in brain targeting drug delivery system by nasal route. J Control Release 2017;268:364–89.
[16] Gao HL. Progress and perspectives on targeting nanoparticles for brain drug delivery. Acta Pharm Sin B 2016;6(4):268–86.
[17] Sun B, Yeo Y. Nanocrystals for the parenteral delivery of poorly water-soluble drugs. Curr Opin Solid State Mater Sci 2012;16(6):295–301.
[18] Ullah N, Khan S, Ahmed S, Govender T, Faidah HS, de Matas M. Dexibuprofen nanocrystals with improved therapeutic performance: fabrication, characterization, in silico modeling, and *in vivo* evaluation. Int J Nanomedicine 2018;13:1677–92.
[19] Wang CH, Wang R, Cheng XM, He YQ, Wang ZT, Wu C, et al. Comparative pharmacokinetic study of paeoniflorin after oral administration of decoction of Radix Paeoniae Rubra and Radix Paeoniae Alba in rats. J Ethnopharmacol 2008;117(3):467–72.
[20] Zhu GW, Zhang GJ, Wang M, Wang JJ, Zeng WX, Gao XM. Simultaneous determination of nine active compounds of the traditional Chinese medicinal prescription shaoyao-gancao-tang and analysis of the relationship between therapeutical effect and compatibility of medicines. Evid Based Complement Alternat Med 2014;2014:521038.
[21] Steiner RA, Tucker JA. Keep it together: restraints in crystallographic refinement of macromolecule-ligand complexes. Acta Crystallogr D Struct Biol 2017;73(Pt3):93–102.
[22] Zhou H, Wang CZ, Deng T, Tao R, Li WJ. Novel urushiol derivatives as HDAC8 inhibitors: rational design, virtual screening, molecular docking and molecular dynamics studies. J Biomol Struct Dyn 2018;36(8):1966–78.
[23] Pangeni R, Sharma S, Mustafa G, Ali J, Baboota S. Vitamin E loaded resveratrol nanoemulsion for brain targeting for the treatment of parkinson's disease by reducing oxidative stress. Nanotechnology 2014;25(48):485102.
[24] Muntimadugu E, Dhommati R, Jain A, Challa VG, Shaheen M, Khan W. Intranasal delivery of nanoparticle encapsulated tarenflurbil: a potential brain targeting strategy for Alzheimer's disease. Eur J Pharm Sci 2016;92:224–34.
[25] Witschi C, Mrsny RJ. *In vitro* evaluation of microparticles and polymer gels for use as nasal platforms for protein delivery. Pharm Res 1999;16(3):382–90.
[26] Wang S, Chow MSS, Zuo Z. An approach for rapid development of nasal delivery of analgesics—dentificationof relevant features, *in vitro* screening and *in vivo* verification. Int J Pharm 2011;420(1):43–50.
[27] Bharatwaj B, Dimovski R, Conti DS, da Rocha SR. Polymeric nanocarriers for transport modulation across the pulmonary epithelium: dendrimers, polymeric nanoparticles, and their nanoblends. AAPS J 2014;16(3):522–38.
[28] Zhu XB, Zeng XW, Zhang XD, Cao W, Wang YL, Chen HJ, et al. The effects of quercetin-loaded PLGA-TPGS nanoparticles on ultraviolet B-induced skin damages *in vivo*. Nanomedicine 2016;12(3):623–32.
[29] Costa P, Sousa Lobo JM. Modeling and comparison of dissolution profiles. Eur J Pharm Sci 2001;13(2):123–33.
[30] Xu XJ, Appel EA, Liu X, Parker RM, Scherman OA, Abell C. Formation of cucurbit[8]uril-based supramolecular hydrogel beads using droplet-based microfluidics. Biomacromolecules 2015;16(9):2743–9.
[31] Zhang L, Du SY, Lu Y, Liu C, Tian ZH, Yang C, et al. Puerarin transport across a Calu-3 cell monolayer – an *in vitro* model of nasal mucosa permeability and the influence of paeoniflorin and menthol. Drug Des Devel Ther 2016;10:2227–37.
[32] Li FJ, Zhu AP, Song XL, Ji LJ, Wang J. The internalization of fluorescence-labeled PLA nanoparticles bymacrophages. Int J Pharm 2013;453(2):506–13.
[33] Nour SA, Abdelmalak NS, Naguib MJ, Rashed HM, Ibrahim AB. Intranasal brain-targeted clonazepam polymeric micelles for immediate control of status epilepticus: *in vitro* optimization, *ex vivo* determination of cytotoxicity, *in vivo* biodistribution and pharmacodynamics studies. Drug Deliv 2016;23(9):3681–95.